Energetic landscape and terminal emitters of phycobilisome cores from quantum chemical modeling

Lorenzo Cupellini,[a,*] Michal Gwizdala[b,c,d], Tjaart Krüger[b,c,e]

[a] *Dipartimento di Chimica e Chimica Industriale, Università di Pisa, Via G. Moruzzi 13, 56124 Pisa, Italy*

[b] *Department of Physics, University of Pretoria, Lynnwood Road, Pretoria, 0002, South Africa*

[c] *Forestry and Agricultural Biotechnology Institute (FABI), University of Pretoria, Lynnwood Road, Pretoria, 0002, South Africa*

[d] *Present address: ICFO - Institut de Ciencies Fotoniques, The Barcelona Institute of Science and Technology, Castelldefels 08860, Spain*

[e] *National Institute of Theoretical and Computational Sciences (NITheCS) South Africa*

[*] *Corresponding author. Email: lorenzo.cupellini@unipi.it*

Abstract

Phycobilisomes (PBs) are giant antenna supercomplexes of cyanobacteria that use phycobilin pigments to capture sunlight and transfer the collected energy to membrane-bound photosystems. In the PB core, phycobilins are bound to particular allophycocyanin (APC) proteins. Some phycobilins are thought to be terminal emitters (TEs) with red-shifted fluorescence. However, the precise identification of TEs is still under debate. In this work, we employ multiscale quantum-mechanical calculations to disentangle the excitation energy landscape of PB cores. Using the recent atomistic PB structures from Synechoccoccus PCC 7002 and Synechocystis PCC 6803, we compute the spectral properties of different APC trimers and assign the low-energy pigments. We show that the excitation energy of APC phycobilins is determined by geometric and electrostatic factors, and is tuned by the specific protein-protein interactions within the core. Our findings challenge the simple picture of a few red-shifted bilins in the PB core and instead suggest that the red-shifts are established by the entire TE-containing APC trimers. Our work provides a theoretical microscopic basis for the interpretation of energy migration and time-resolved spectroscopy in phycobilisomes.

1 Introduction

The phycobilin pigments of phycobilisomes (PBs) absorb light and transfer the excitation energy first within the PBs and eventually to the chlorophylls of nearby photosystems.[1] The phycobilins are linear tetrapyrrole pigments that bind covalently to water-soluble phycobiliproteins. The phycobiliproteins determine their geometry, physicochemical microenvironment, locations, and relative orientations, the combination of which determines their specific role within the PB complex. Multiple phycobiliprotein complexes and linker proteins assemble into large PB complexes. The macromolecular structure of PBs can vastly differ — depending on the strain of cyanobacteria or algae — or can adjust to environmental conditions.[2–4]

While high-resolution PB structures were unavailable until only recently, the overall arrangement of phycobiliproteins within PB complexes and the X-ray crystal structures of individual phycobiliproteins subunits have been reported over the past few decades.[5–9] In many hemidiscoidal cyanobacterial phycobilisomes, most pigments bind to the phycocyanin (PC) rods.[6] When isolated, PC rods emit around 650 nm, although red-shifted emission was also reported for these complexes.[10,11] The rods typically surround a central core within the PB complex. The core is always composed of either 2, 3, or 5 allophycocyanin (APC) cylinders, depending on the organism.[12]

In the model cyanobacteria *Synechoccoccus* PCC 7002 and *Synechocystis* PCC 6803 (hereafter **Sco. 7002** and **Scy. 6803**, respectively), the PB core is composed of 3 parallel APC cylinders, each containing 4 toroidal trimers.[13,14] Most trimers are composed of three identical ApcA/ApcB heterodimers and here we refer to them as **AB-trimers**. Both subunits, ApcA and ApcB, bind a single phycobilin pigment, the phycocyanobilin (PCB). Despite binding the same type of phycobilin pigment as the PC rods, the **AB-trimers**' emission peaks at around 660 nm, i.e., ∼10 nm red-shifted compared to PC.

While the top cylinder of the core (T in Fig. 1a) consists exclusively of AB-trimers (along with a few non-pigmented linker proteins and protein domains), in each of the basal cylinders (B1 and B2 in Fig. 1a) the position of two AP-trimers is occupied by two other types of trimers, namely, D- en EF-trimers, which exhibit emission red-shifted to ∼680 nm and are therefore are referred to as the terminal emitters (TEs). These TE trimers have a different apoprotein composition than AB-trimers (Fig. 1b-d). In the **D-trimer**, one of the ApcA subunits (1 out of 3) is replaced by a product of a different gene, the ApcD subunit (Fig. 1h), while in the **EF-trimer**, an ApcA subunit of one heterodimer and an adjacent ApcB subunit of a neighboring heterodimer are replaced by ApcE and ApcF, respectively.[13–15] While ApcD and ApcF resemble

ApcA and ApcB, respectively, ApcE (also known as L_{CM}) comprises an ApcA-like domain as well as linker-protein domains that are critical for the integrity of the PB complex and its attachment to the thylakoid membrane. PCB is the only type of pigment bound by the PBs of **Sco. 7002** and **Scy. 6803**, including their TEs. According to the current functional models of PB complexes, the TEs collect excitation energy from other pigments in the PB complex and transfer it to the membrane-bound photosystems that host the photosynthetic reaction centers. Effectively, the PC rods, APCs, and TEs form an energy ladder that defines the flow of excitations in PBs, from the distal sites to the central core and subsequently to the reaction centers.

The physiological role of PBs depends largely on the significant red-shifted absorption and emission of some of its PCB pigments. However, there is no consensus about the molecular origin of this spectroscopic heterogeneity. Various mechanisms have been proposed to explain the red-shifts,[1] the most prominent being (i) excitonic interactions between the pigments in the core,[12,16,17] (ii) modification of the pigments' microenvironment during the formation of the APC core,[17] (iii) a change in the geometry of the pigments,[8] or a combination of these mechanisms. The challenge to explain the origin of the red-shifts in the TEs is somehow aggravated by the fact that studies involving cyanobacterial mutants have shown that the effects of replacing some of the TE trimers with **AB-trimers** are dissimilar in PBs from **Sco. 7002** and **Scy. 6803**.[18–20] In particular, the replacement of a **D-trimer** does not change the emission at 77 K in **Sco. 7002** while it blue-shifts the emission from **Scy. 6803** PBs. An opposite effect for these strains was reported for PBs lacking the ApcF subunit, with only minor changes in emission at 77 K in **Scy. 6803** and a more substantial blue-shift in **Sco. 7002** PBs. In addition, the TEs in different strains may also have different physiological functions in the regulatory processes of photosynthesis such as state transitions.[21]

Recently, two cryo-EM structures have been resolved for the cyanobacterial PB at near-atomic resolution. Zheng *et al.* reported the structure from **Sco. 7002** at 3.5 Å resolution,[14] along with the structure from *Anabaena* 7120 at 3.9 Å resolution. Later, Domínguez-Martín *et al.* reported the structure of the PB from **Scy. 6803** at a 2.8 Å resolution for the PB core.[13] These structures hold the promise of identifying the location of the TEs and explaining the structural origin of the red-shifted emission.

The PCB binding pockets of the different APC variants are remarkably similar (Fig. 1e-i), with the exception of ApcE. The pyrrolic hydrogens of rings B and C are coordinated by the negatively charged Asp84 (in ApcA/ApcB numbering), which, in turn, makes a salt bridge with Arg83. Tyr116 completes the interaction on the other side of the pyrrolic rings in all APCs except for ApcE. In ApcD and ApcE, a tryptophan is present (Trp87 in ApcD), but only in ApcE this Trp is parallel to the D-ring of the PCB. Finally, the ApcE-bound PCB presents a peculiar *ZZZssa* geometry, that is, the conformation of the angle between rings A and B is opposite to all the other PCBs.[9] This is made possible by the position of Cys186 that covalently attaches the chromophore to the protein (Fig. 1g).

In APC trimers, the PCB binding pockets are generally completed by a few residues of the other protomer chain, which are in contact with the D-ring of the pigment. For the ApcA-like (i.e., α-) chains, these are residues 74-76 of the ApcB-like (i.e., β-) chain belonging to a different heterodimer.

Atomistic and quantum chemical investigations have allowed unprecedented insights into the exciton structure of light-harvesting complexes.[22–24] However, studies on phycobiliproteins have been mostly focused on the antenna complexes of cryptophytes.[25–27]

In this study, we aim to identify the TE sites in cyanobacterial PBs of **Sco. 7002** and **Scy. 6803** and to understand similarities and differences between the two species. To do so, we employ state-of-the-art multiscale quantum-mechanical (QM) calculations and simulations of the spectroscopic properties. First, we analyze the exciton structure of the PB core by means of fully polarizable multiscale calculations that take into account the impact of the protein environment on the structure and on the transition properties of the pigments. Thereafter, we employ spectral simulations to understand the origin of the low-lying emitting states in the PBs. Finally, we simulate the excitation energy transfer (EET) pathways within the PB core, which allows us to follow the transport of excitations to the TEs.

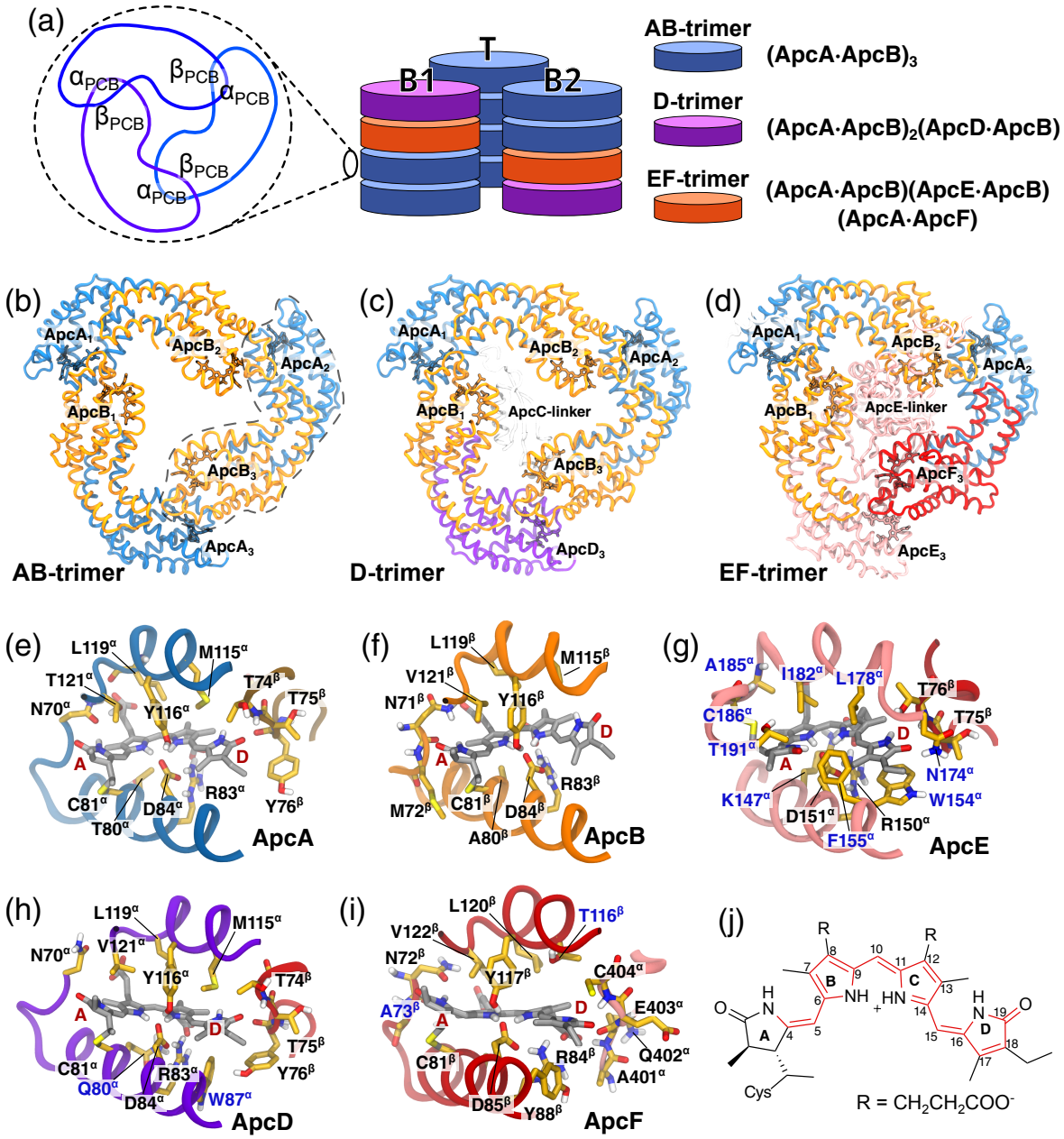

Figure 1 Organization of the PB core and pigment binding pockets. (a) Organization of the PB core. One top (T) and two bottom (B1/B2) cylinders are each composed of four trimers, represented in different colors. The scheme on the left schematically shows the protomer composition of one trimer and the approximate position of α and β pigments. (b-d) The three different APC trimers found in the PB core. One of the $\alpha\beta$ protomers is highlighted in (b) with a dashed line. Labeling of the Apc apoproteins in each trimer does not follow the protomers but rather the closely spaced pigment dimers. The α-like chains are shown in blue (ApcA), violet (ApcD), and pink (ApcE), and the β-like chains are shown in orange (ApcB) or red (ApcF). The linker protein ApcC and the linker domain of ApcE (ApcE-linker) are also shown. (e-i) Binding pockets of the PCB in the different Apcs. The panels show ApcA (e) and ApcB (f) from the **AB-trimer**, ApcE (g), ApcD (h), and ApcF (i). Residues within ~3 Å of the PCB rings are shown and labeled according to the chain (α-like or β-like). The location of rings A and D of the PCB is labeled in red and is consistent in all panels. The residues that differ in ApcD/ApcF/ApcE from the parent ApcA or ApcB chain are labeled in blue. (j) Chemical structure of PCB, with labeling of the four pyrrole rings. The conjugation pattern is highlighted in red. The structures in panels (b-i) are those of **Sco. 7002** PB (PDB: 7EXT) as refined in the present work (see Methods).

2 Results

2.1 Multiscale QM/MM calculations

During APC trimerization, closely spaced PCB dimers are formed with ∼11 Å edge-to-edge distance, suggesting excitonic interactions among PCBs. This observation, coupled with the close interaction between Apc apoproteins within each trimer, prompted us to consider trimers as building blocks of the core cylinders. We thus focused our attention on the three functionally and structurally different trimers found in the PB core (Fig. 1): the **AB-trimer** $(ApcA{\cdot}ApcB)_3$, the **D-trimer** $(ApcA{\cdot}ApcB)_2(ApcD{\cdot}ApcB)$, and the **EF-trimer** (ApcA·ApcB)(ApcE·ApcB)(ApcA·ApcF), and did not consider other linker chains in these calculations.

To obtain a comparison as fair as possible between structures of different resolution, we employed a MM + QM/MM refinement procedure, as detailed in the Methods section. Thereafter, we calculated the site energies and exciton couplings among all the six pigments in each trimer. This strategy was validated on the $(ApcD/ApcB)_3$ trimer resolved by Peng *et al.*[8] (PDB: 4PO5) at a 1.75 Å resolution (see Section S1 in the SI).

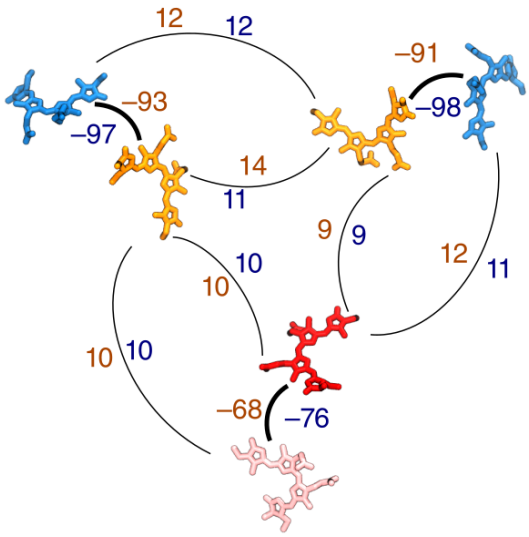

Figure 2 Excitonic couplings within the **EF-trimer**. All values are in cm^{-1}, and couplings less than 5 cm^{-1} are not shown. Orange numbers refer to **Sco. 7002** while blue numbers refer to **Scy. 6803**. The orientation and colors of the PCB pigments are the same as in Figure 1d.

Exciton couplings and site energies

The strongest coupling among PCBs predictably occurs between the closely spaced pigment dimers, in all the considered trimers. Figure 2 shows the largest couplings in the **EF-trimer**, for which strong exciton couplings have been hypothesized.[1] The largest couplings occur in the closely spaced ApcA/ApcB pigment dimers and amount to ∼100 cm^{-1}. However, the coupling between ApcE and ApcF is slightly smaller (∼70 cm^{-1}). This is the only exception, because 90–100 cm^{-1} couplings are found for all the remaining pigment dimers in the **AB-trimer**, as well as in the **D-trimer** and **EF-trimer** (Table S2).

These couplings calculated here are much smaller than the largest ones computed for "closed" PC biliproteins of cryptophytes,[25,27] but are still expected to influence the exciton structure of the trimers. Womick and Moran have assumed exciton couplings of around 150 cm^{-1} to investigate vibronic excitons in Apc trimers.[28] Our calculations show that these couplings are smaller than initially predicted, although of a similar order of magnitude. While these couplings are of the same order as the medium-to-strong couplings in the light-harvesting complexes of plants,[29,30] they can support delocalization at most within the PCB dimers.

Next, we computed the site energies of the core pigments in the two structures of the PB core. We first focus on the

AB-trimer, which does not contain TE pigments. Comparison of the **Sco. 7002** and **Scy. 6803** trimers, however, reveals a striking difference between the two structures (Fig. 3, left): the site energies of **Sco. 7002** follow a regular pattern, where the ApcB pigments lie energetically above the ApcA pigment by ∼0.11 eV (∼900 cm^{-1}). Conversely, **Scy. 6803** follows a more erratic pattern with no clear ApcA/ApcB difference, although the lowest-lying pigment is bound to ApcB. To explain this difference, we repeated the calculations *in vacuo*, while retaining the internal structure of the PCBs. The overall picture is the same in these calculations, indicating that most of the differences arise from the internal geometry of the pigments.

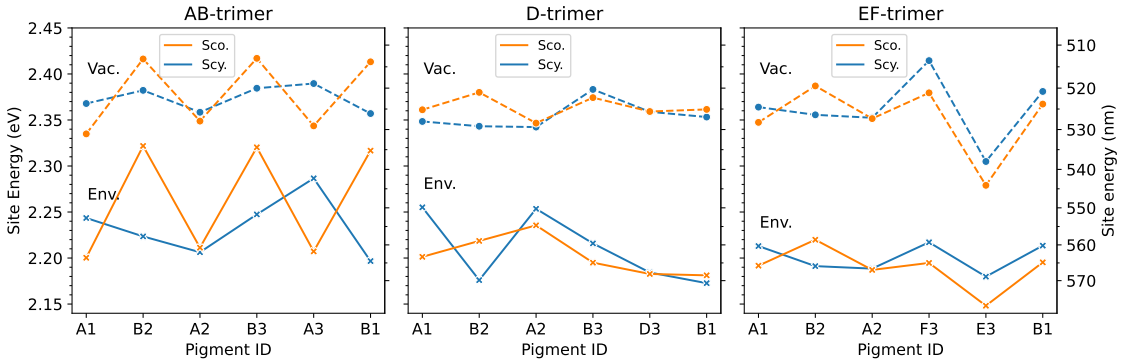

Figure 3 Energy ladder in the APC trimers. Site energies calculated in environment (Env.) are compared to those calculated *in vacuo* (Vac.). Orange data refers to **Sco. 7002** while the blue data refers to **Scy. 6803**. Each APC is labeled according to Figure 1b-d. Data points are connected by lines for better visibility.

We next investigated the two TE trimers (Fig. 3, middle and right). Compared to the **AB-trimer**, both of these trimers show significantly lower excitation energies for most pigments. Somewhat surprisingly, the pigments bound to ApcD (D3), ApcE (E3), or ApcF (F3) are not the only red-shifted ones. Instead, they have similar excitation energies to the other ApcA/ApcB pigments in the same trimer, with the exception of ApcE in **Sco. 7002**. In particular, ApcF is not among the low-energy pigments, whereas ApcE is the lowest-energy pigment only in **Sco. 7002**. Conversely, ApcB pigments are substantially red-shifted in both the **D-trimer** and **EF-trimer** with respect to the **AB-trimer**. The only exceptions are the ApcA pigments in the **D-trimer** of **Scy. 6803**, which have similar excitation energies to the blue-most pigments of the **AB-trimer**.

Origin of the site energy ladder.

In order to understand the difference in site energy among bilins of different trimers, we analyzed the relationship between structural distortion and excitation energy.[9,31,32] Figure 4a shows that the *in vacuo* excitation energy is clearly correlated with the dihedral angle N_C=C_{14}-C_{15}=C_{16} between rings C and D of the bilin. The only clear outliers are the ApcE pigments, which present an *s-cis* configuration for the dihedral connecting rings A and B. A similar dependence of the excitation energy with the D-ring torsion could be deduced from a torsional scan of PCB *in vacuo* (see Fig. S3).

A more refined analysis of geometrical parameters (Section S2 in the SI) revealed that the excitation energy is influenced by the linear angle between rings B and C, namely C_9-C_{10}-C_{11}, as well as the dihedral angle between rings A and B. However, the latter angle does not seem to explain much of the remaining variability, given the small coefficients associated with the fitting.

The differences in these few geometrical parameters are determined by the steric and electronic effects of the Apc pockets. Overall, these structural differences give rise to a site energy spread of about 0.06 eV (or 500 cm^{-1}) for both ApcA and ApcB pigments, most of which is directly related to the D-ring dihedral. Additional variability is given by the electrochromic effect of the environment (Fig. 4b). Although the excitation energy of PCBs in environment is well correlated to that *in vacuo*, Figure 4b shows that not all PCBs are shifted the same by the environment. On average, ApcB-type pigments (including ApcF) are red-shifted more than ApcA-like pigments. Overall, the protein environment is directly responsible for an additional ∼0.07 eV variability in the site energy of either ApcA-like or ApcB-like pigments.

To further analyze the site energy differences among the pigments, we focused on the ApcA protein pockets. In the core trimers, the ApcA bilin is also in contact with the ApcB amino acid residues of a neighboring $\alpha\beta$ protomer that "close" the

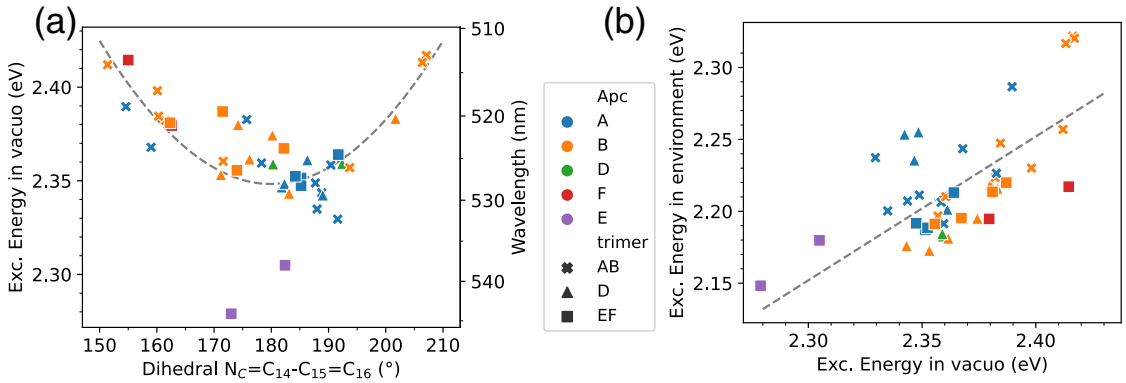

Figure 4 (a) Relationship between the N_C=C_{14}-C_{15}=C_{16} dihedral angle (see Fig. 1j) and the excitation energy *in vacuo*. Different colors refer to different Apc apoproteins, whereas different symbols refer to different trimers (see Fig. 1b-d). Data from both **Sco. 7002** and **Scy. 6803** was used. The dashed line is a fit of the function $f(\phi^{CD}) = A + B\left(1+\cos(\phi^{CD})\right)$, with parameters $A = 2.348$ eV, $B = 0.571$ eV, and ϕ^{CD} the dihedral angle. (b) Correlation between the excitation energy *in vacuo* and in the protein environment. The dashed line shows a constant offset $y = x - 0.148$ eV as a guide to the eye.

protein pocket. Figure S4 shows a superposition of ApcA pockets from two **AB-trimers** (one from the top cylinder and one from a bottom cylinder) and the **D-trimer** of **Scy. 6803**. There appears to be a substantial variability in the position and orientation of several side chains of both ApcA and ApcB. It is difficult to infer a single factor in the protein pocket determining the site energy. Nonetheless, we can note that in the pockets that give rise to a blue-shifted ApcA site energy, residues are found generally further from the pigment, leaving more room for the D-ring to move. Conversely, a tighter pocket likely constrains the bilin in a more planar configuration, possibly reducing the excitation energy. It is difficult to perform a complete analysis on all residues; however, we show in Figure S5 that the torsion between rings C and D is generally correlated with the distance to Tyr88 in the binding pocket. A larger distance, namely more freedom for ring D to move, is correlated with a larger deviation from planarity. Nonetheless, many factors within the binding pocket can concur in determining the geometry of the bilin.

Contrary to **Scy. 6803**, the **Sco. 7002** structure presents identical pockets for the ApcA subunits in the AB-trimer. The ApcA structures in the **D-trimer** are different but again identical to each other. This strongly suggests that some symmetry was imposed by Zheng *et al.* [14] in the final atomistic model, which was not the case for the **Scy. 6803** structure of Ref. 13. Substituting the various conformations of the Apc proteins in the PB core by an average structure likely results in a less disordered but less realistic structure for **Sco. 7002**. Unfortunately, this discrepancy between the two PB structures does not allow for an unbiased comparison between the two species. However, this issue does not prevent us from simulating the spectral and energy transfer properties of the PB core in the two species. In particular, while the average energies in the **AB-trimer** of **Sco. 7002** seem noticeably shifted, in the TE trimers the site energies of the two species are much more similar.

2.2 Spectral properties

We are now in a position to simulate the absorption spectra of the trimers and of the entire PB core. The spectrum of the core can be well approximated by a weighted sum of the constituting trimers (see Fig. S7) assuming two **EF-trimers**, two **D-trimers**, and eight **AB-trimers**. To better resolve the spectral features, all spectra were computed at 77 K.

Simulated spectra show red-shift of TE trimers.

The spectra simulated at 77 K are shown in Figure 5a,b (dark brown lines). To achieve a meaningful comparison with experiments, we employed a rigid shift (-2100 cm^{-1}) for all calculated spectra, which takes into account all systematic errors from the calculations.[24] The shift parameter was determined independently on the $(\text{ApcD/ApcB})_3$ trimer from **Scy. 6803** (see Section S1 in the SI), which allowed us to avoid overfitting this parameter to the experiments. The absorption spectra present a main absorption band at $\sim$660 nm, close to the expected absorption maximum of the isolated PB core.[33]

Figure 5 also shows the contribution from each trimer in the core. The **AB-trimers** determine most of the absorption

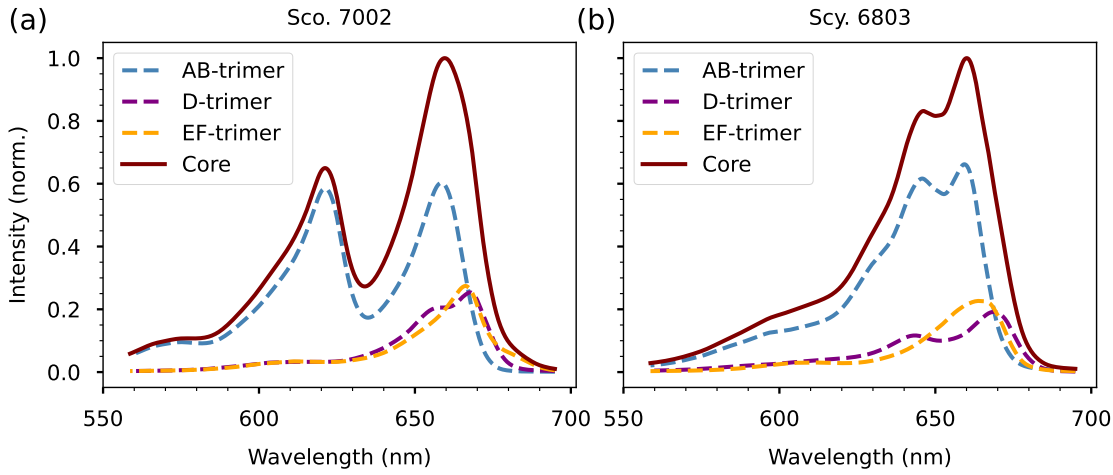

Figure 5 Simulated absorption spectra for the PB core of (a) **Sco. 7002** and (b) **Scy. 6803**. The core spectra are shown as dark brown lines. The contributions of each trimer type are shown as dashed lines. The spectra were all red shifted systematically by -2100 cm^{-1}.

spectrum, as they account for two-thirds of the pigments, whereas the TE trimers contribute mainly to the red edge. As expected, the spectrum of the TE trimers is red-shifted with respect to the lowest-energy band from the rest of the PB core. The red wings of the spectra indicate that the TE trimers absorb at wavelengths in the region around 680 nm where the **AB-trimers** do not contribute.

Comparison of the spectra of **Sco. 7002** and **Scy. 6803** in Figure 5a,b reveals a substantial discrepancy between the two species. Specifically, the spectrum of **Sco. 7002** presents a strong blue-shifted APC band at around 620 nm, which in **Scy. 6803** is much closer to the main band. This band originates from the significantly blue-shifted ApcB in the **AB-trimer** of **Sco. 7002** (Fig. 3, left). The presence of a blue-shifted band is consistent with the absorption spectra measured for the **Sco. 7002** 18S subcore preparation, which indeed show a significant shoulder at $\sim$600 nm[18], albeit much less pronounced. However, in Ref. 18 the intensity of this shoulder varied significantly between preparations. Although the **Scy. 6803** simulated spectrum also shows a small shoulder around 600 nm, it is the vibronic sideband of the peaks at $\sim$650 nm. In our **Sco. 7002** model, the blue-shifted band is quite sharp because all ApcBs have the same site energies. A more realistic distribution of site energies would result in a broader, less prominent band. Overall, the experimental evidence supporting the blue-shifted ApcB band in **Sco. 7002** is not sufficiently clear.

In addition to the differences at the blue edge of the spectrum, it is noteworthy that **Sco. 7002**'s spectrum has a more pronounced red edge, with both the **D-** and **EF-trimers** having significant absorption. Conversely, in **Scy. 6803**, the **D-trimer** contributes more to the very red edge of the spectrum. These differences arise from the site energies of the TE trimers (Fig. 3), which are different in the two species. Curiously, even though the differences between the site energies are relatively small, they visibly influence the absorption spectrum.

Fluorescence simulations

Next, we simulated the fluorescence spectra of each TE trimer in the core (Fig. 6). We first focus on the **D-trimer**, which in our simulations shows an emission maximum at 671 nm and 676 nm for **Sco. 7002** and **Scy. 6803**, respectively. Mutational analysis of both cyanobacterial species has shown that the removal of ApcD does not visibly change the fluorescence spectrum.[18,20] To investigate this effect, we performed *in silico* mutational analysis by constructing a model of ΔApcD. To better capture the effect of the mutation, in our ΔApcD model the ApcD site energy is increased to match the site energy of the ApcA and ApcB pigments with the highest energy. In these models of ΔApcD, the fluorescence maximum remains essentially unchanged (Fig. 6a,d). This is consistent with our finding in Figure 3 that the ApcD pigment is not the lowest-energy pigment in the **D-trimer**. This result is in agreement with the mutational analysis of Refs.[18,20], independent of whether the **D-trimer** is the lowest TE in the core. In fact, even after substituting ApcF with ApcB, the removal of ApcD does not impact the emission wavelength in these experiments. This can only be true if ApcD itself is not the lowest-energy pigment in the **D-trimer**.

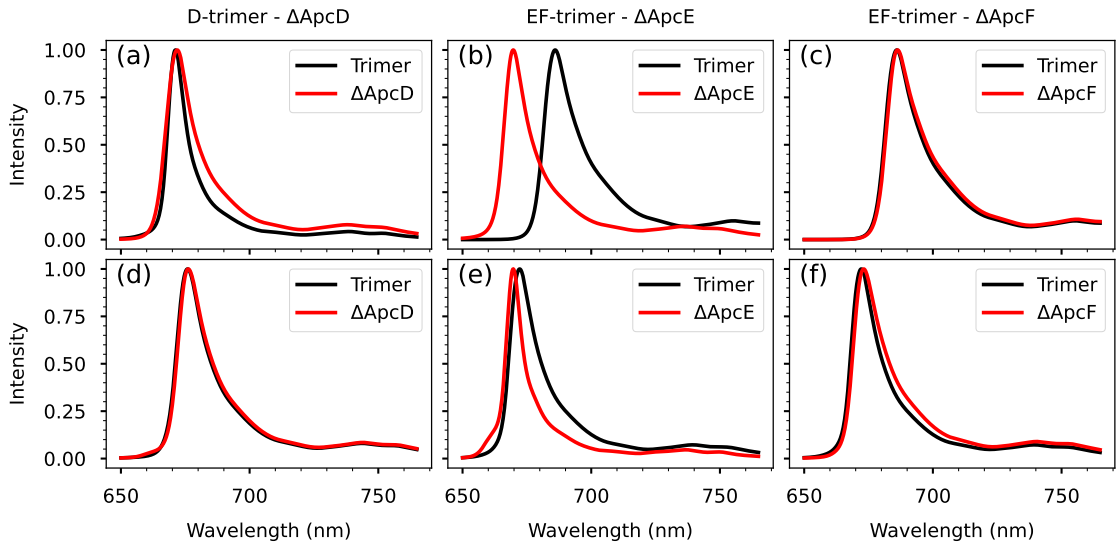

Figure 6 Simulated 77 K fluorescence spectra of individual APC trimers in **Sco. 7002** (a-c) and **Scy. 6803** (d-f). (a,d) **D-trimer** and the corresponding ΔApcD mutant. (b,e) **EF-trimer** and the corresponding ΔApcE mutant. (c,f) **EF-trimer** and the corresponding ΔApcF mutant. Models for the mutants were obtained by changing the site energy of the bilin bound to the deleted apoprotein, except for ΔApcE, in which the bilin was removed (see text). The spectra were all shifted systematically by -2100 cm^{-1}.

The **EF-trimer** shows a different emission behavior between **Sco. 7002** and **Scy. 6803** (Fig. 6b,e). Consistent with the site energies (Fig. 3), the fluorescence of **Sco. 7002** is red-shifted with a peak at around 686 nm, whereas the **Scy. 6803 EF-trimer** emits at around 672 nm. Considering also the emission wavelengths of the **D-trimer**, these results indicate an overall fluorescence at around 676 nm for our **Scy. 6803** PB model due to the **D-trimer**, and a 686 nm fluorescence for our **Sco. 7002** model due to the **EF-trimer**. Given that the PB emission maximum at 77 K is at 680 nm for both cyanobacterial species, this data provides information about the accuracy of our site energy estimates. Considering both the **D-** and **EF-trimers**, the lowest site energy of **Scy. 6803** is likely overestimated by 100–180 cm^{-1} (0.01–0.02 eV) in the calculations. Likewise, the lowest site energy of **Sco. 7002** is probably underestimated by roughly the same amount. These errors are smaller than the relative variability in the site energies of both species (Fig. 3). We remark that the systematic error in site energies due to our quantum chemical methods was removed in these simulations by applying a -2100 cm^{-1} shift to the simulated spectra.

To better understand the fluorescence properties of the **EF-trimers**, we considered the ApcE-C180S mutation, which essentially removes the ApcE bilin,[18,20,34] and modeled this mutant by simply removing the ApcE pigment from the exciton system of the **EF-trimer**. For consistency, we name this mutation ΔApcE. The ApcE-C180S mutation is known to cause a blue shift of ∼7 nm, or about 150 cm^{-1}. Our simulations qualitatively confirm that ApcE removal results in a blue shift for both species. However, the calculated shift is only 60 cm^{-1} for **Scy. 6803** and more than 300 cm^{-1} for **Sco. 7002**, confirming our suspicion that the site energy of ApcE is underestimated in the calculations on **Sco. 7002** and overestimated in **Scy. 6803**.

Curiously, the simulated ΔApcE emission maximum is the same in the two species (red spectra in Fig. 6b,e). The maxima are around 670 nm, which is at a higher energy than the **D-trimer** emission discussed above. Therefore, in ΔApcE mutants, the **D-trimer** would be the lowest-energy emitter. Our results on the **D-trimer** thus predict that ΔApcE of **Scy. 6803** would have an emission maximum around 676 nm, which is consistent with experimental results. Conversely, the ΔApcE mutant of **Sco. 7002** would show an emission maximum at 672 nm, which is slightly too high. This comparison suggests that the site energies calculated for the **D-trimer** of **Scy. 6803** are accurate, whereas those of **Sco. 7002** are somewhat overestimated. In any case, we conclude that the main emission wavelength observed in ΔApcE mutants corresponds to the emission of the **D-trimer**, which is expected at around 675 nm in both species. In contrast, in the wild-type PB, the lowest-energy emission at around 680 nm arises from the ApcE pigment.

Finally, we investigate the effect of ApcF deletion. Like for ΔApcD, ΔApcF was modeled by increasing the ApcF site energy. Removal of ApcF does not significantly affect the emission in either species (Fig. 6c,f), in stark contrast to the experimental

results on both species.[18,20] This result was expected, given that ApcF is not red-shifted in either PB (Fig. 3). Remarkably, for ΔApcF to have any effect on the emission, this pigment should have roughly the same energy as ApcE, i.e., 0.04 eV lower in energy. This discrepancy is larger than the errors estimated for the other pigments. Notably, in ΔApcF PBs, an ApcB protein supposedly takes the place of ApcF. This means that the residues surrounding the ApcE pigment-binding pocket are changed. Indeed, at the interface, ApcF and ApcB have different sequences (see Fig. S8). Furthermore, several ApcE side chains (including W154) would need to rearrange if ApcF was substituted with ApcB because of the ensuing clashes (Fig. S8). We conclude that the change in the interface with ApcE when ApcF is substituted by ApcB is the cause for the emission blue shift in ΔApcF PBs.

2.3 Energy transfer and equilibration in the core

We finally employed our models to investigate the EET dynamics in the PB core. To this end, we reconstructed the exciton Hamiltonian of the entire core combining the site energies and couplings calculated for each trimer with inter-trimer couplings calculated with the TrEsp method.[35] Thereafter, we simulated the EET dynamics at room temperature using the Generalized Förster method, where all closely associated bilin dimers were defined as exciton domains. We started our simulations by homogeneously populating the top cylinder and then followed the total population of the **AB-**, **D-**, and **EF-trimers**.

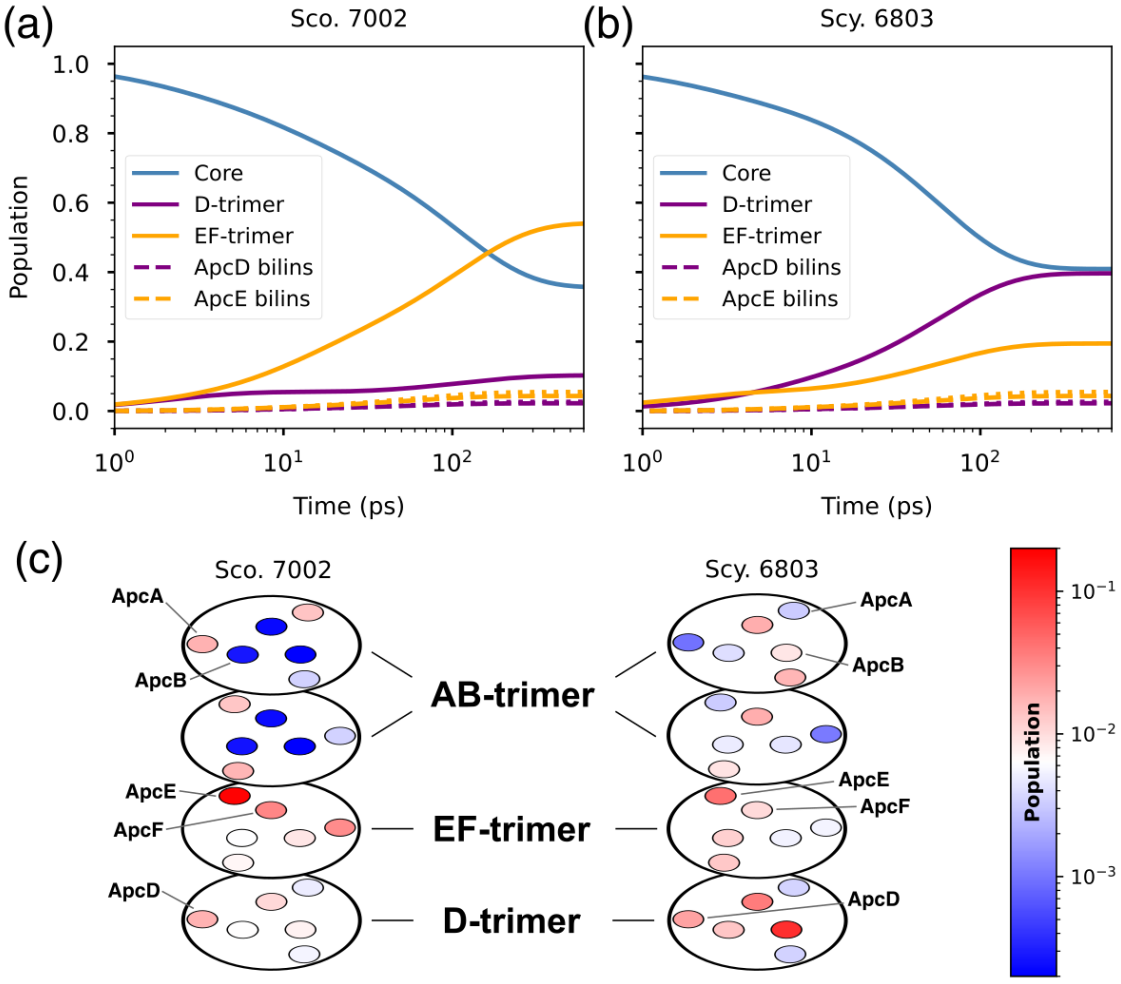

Figure 7 Excitation energy transfer dynamics of (a) **Sco. 7002** and (b) **Scy. 6803**. The light blue "Core" lines show the combined population of all non-TE trimers (**AB-trimers**), whereas the purple and orange solid lines represent the total population of **D-** or **EF-trimers** in both cylinders. The dashed lines represent the population of single ApcD or ApcE pigments. (c) Distribution of the final population (at 500 ps) in one of the bottom cylinders. Each trimer is represented schematically as a disk, while the circles inside represent the bilins with their final excited-state populations depicted by color. Red/blue colors represent large/small populations, respectively, on a logarithmic scale.

Simulations of EET show ∼100 ps transfer to the TE trimers. The EET population dynamics of the PB cores are shown in Figure 7a and b for **Sco. 7002** and **Scy. 6803**, respectively. The overall energy-transfer dynamics are similar in the two cases, with the core transferring energy to both TE trimers. The characteristic EET time from the core to the trimer is around 100 ps for **Sco. 7002** and 60 ps for **Scy. 6803**, as fitted from the decay of the non-TE population, and the population is completely equilibrated within 500 ps. The EET times are roughly in agreement with the core equilibration time constants (111–118 ps) extracted from time-resolved fluorescence of unquenched PBs.[36,37] The slower EET time predicted for **Sco. 7002** arises from the larger average energy gap between ApcA and ApcB pigments and with the TE pigments.

Different equilibrium populations of pigments in Sco. 7002 and Scy. 6803. At equilibrium, roughly 60% of the excited-state population ends up in either of the TE trimers, in both **Sco. 7002** and **Scy. 6803**. However, the individual populations of the trimers are substantially different in the two cases. In **Sco. 7002**, a large part of the TE population is on the ApcE pigments of the bottom cylinders. Conversely, in **Scy. 6803**, only 10% of the total population ends up on the ApcE pigments, whereas the majority of the TE population is shared among the pigments of the **D-trimer**. This is exemplified in Figure 7, where we show the spatial distribution of the excited-state population for one bottom cylinder. These differences directly arise from the different site energies of the TE trimers, as in our model of **Sco. 7002** PB, ApcE is by far the lowest-energy pigment, whereas in **Scy. 6803**, several pigments have similar energies on the red side of the energy ladder. In both species, however, there is a substantial population on the ApcA and ApcB pigments of the TE trimers, which is in contrast to the general assumption that there are only two or three TE pigments in each bottom cylinder of the PB.[1]

3 Discussion

Substantial differences in cryo-EM structures may be artifacts.

The two recent structures[13,14] of the PB core investigated in this work present substantial differences already in the **AB-trimer**. The regular pattern of site energies obtained in **Sco. 7002** (Fig. 3) likely arises from the symmetries imposed within the **AB-trimer** structure in 7EXT. This is clearly not the case for the 7SC7 structure of **Scy. 6803**, where a significant variability is found between different pockets (Fig. S4). More strikingly, calculations based on the **Sco. 7002** structure predict ApcB site energies ∼900 cm^{-1} higher than those of ApcA. This is consistent with single-molecule measurements of isolated APC trimers of *Spirulina platensis*[38], where the ApcA absorption was found to be ∼750 cm^{-1} red-shifted from that of ApcB. However, these measurements also revealed substantial inhomogeneity in the excitation energies of the pigments. From the calculations on the **Scy. 6803** (7SC7) structure, we can deduce that this inhomogeneity is present in the intact PB core, for both ApcA and ApcB pigments.

The question arises whether these differences emerge from a genuine dissimilarity between the two cyanobacterial species, or whether they are artifacts of the structural models employed in this work. We stress that the resolution of the cryo-EM maps (2.8 Å for 7SC7 and 3.5 Å for 7EXT) may not be sufficient to precisely pinpoint the atomic positions of the pigments and amino-acid side chains, and some assumptions are necessary to obtain an atomistic model. Unfortunately, this prevents a definitive answer on the origin of the differences between the two species. A possible way to refine the structures, and at the same time sample the pigment-protein conformations that give rise to spectral inhomogeneity, would be to employ molecular-dynamics simulations. However, such simulations are limited both by the quality of molecular-mechanics force fields and by the difficulties in sampling the entire space of pigment-protein configurations[23,24]. In particular, previous work on cryptophyte biliproteins showed that molecular-dynamics structures were not accurate enough for an accurate reproduction of optical properties.[27] On the other hand, advancements in cryo-EM techniques can help improve the accuracy of atomistic models to the level of X-ray structures of single trimers. This will allow a better understanding of the differences in pigment conformations and pocket configurations that occur upon organization of the APC trimers in PB.

Despite the symmetry apparently imposed for the **AB-trimer**, the two TE trimers of **Sco. 7002** show a less regular trend, and on average present more similar site energies to the corresponding pigments of **Scy. 6803**. It is likely that fewer constraints were imposed for these trimers (also because of the lower intrinsic symmetry), which suggests that the **Sco. 7002** results are more reliable for the **D-** and **EF-** trimers.

Red shift in terminal-emitter trimers.

Our calculations show that the pigments of the TE trimers are generally red shifted with respect to those of the **AB-trimer**. Notwithstanding the differences detailed above, this effect is found in both **Sco. 7002** and **Scy. 6803** PBs. The differences are more pronounced for **Sco. 7002**, but in both cases we find that ApcB pigments of both the **D-trimer** and the **EF-trimer** are almost as red-shifted as the TE pigments themselves. This is unexpected, as it is generally assumed that only the TE pigments (i.e., those bound to ApcE, ApcF, and ApcD) are red-shifted [36,39]. On the contrary, our calculations find that ApcF is not as red-shifted as ApcE, and possibly less red-shifted than some ApcB pigments in the same trimer.

Our calculations can also help to explain the red shifts in the TE trimers. First, we can exclude increased excitonic interactions between the pigments in the core. Conversely, the ApcE/ApcF exciton coupling is even slightly smaller than the couplings among the other closely spaced bilins (Fig. 2). The red shifts in TE trimers are instead clearly explained by shifts in site energy of the pigments. These shifts have a geometrical component, which mainly correlates with the distortion of the PCB ring D with respect to ring C. Our calculations in fact show that a more planar geometry of ring D red-shifts the excitation energy of PCBs (Figure 4 and S3), substantiating the mechanism proposed to explain far-red absorption in Apc. [8,31,40,41]. In addition to the geometry, the electrostatic effect of the environment around the bilins further tunes the excitation energies, red-shifting especially the ApcB pigments.

Both structural and electrostatic contributions ultimately originate from the shape and composition of the protein pockets. The formation of APC trimers brings pigments in α-like chains into contact with the β-like chains, which "close" the pocket, affecting the side-chain geometry and the PCB itself. This accounts for the redshift of Apc bilins upon trimerization. [12] Substitution of ApcA or ApcB with their TE analogs can have additional effects on the PCB binding pockets of the remaining ApcA/B, impacting both the geometry of the bound pigments and the electrostatics of their surroundings.

It is worth noting that the ApcB chains in the **EF-trimer** are in contact with the protein-linker domain of ApcE (Fig. 1d). This ApcE-linker is also in contact with the ApcB chains of the **D-trimer** (Fig. S9). It is easy to imagine that these interactions further impact the structure of the PCB-binding pockets in the TE trimers, thus affecting the excitation energies of the pigments. While we have not considered the ApcE-linker explicitly in our calculations, it is clear that the structure of all ApcA/ApcB chains in the **D-trimer** is also determined by the ApcE-linker. The interactions with the ApcE-linker also affect the global structure of the TE trimers. A comparison of the TE trimers with the **AB-trimer** (Fig. S10) shows changes in the relative orientations of ApcA and ApcB in both TE trimers, which effectively depart from the axial symmetry of the trimer. It is thus not unexpected that the PCB-binding pockets are affected as well.

From our calculations, there remains some uncertainty about the identity of the lowest-energy pigments. Nonetheless, combining fluorescence spectra simulations and our *in silico* mutations with the results from mutational analysis [18,20] we could conclude that the ApcE pigment emits at the longest wavelength, whereas multiple pigments in the **D-trimer** can emit at slightly higher energies (i.e., shorter wavelengths). The most surprising result is the site energy of ApcF, which our calculations place to the blue of ApcE, and contributes negligibly to the fluorescence (Fig. 6b,e). In this case, the calculations on both structures agree, which makes this result more robust. As the ΔApcF mutant results in blue-shifted emission, [18,20] we have to conclude that the removal of ApcF affects the nearby ApcE pigment.

Energy equilibration in the core.

Despite the substantial differences in the site-energy ladder of the two PB models, our simulations show that the overall EET to the TEs occurs on similar time scales (60–100 ps, see Fig. 7). The largest difference lies in the final equilibrium, which for the **Sco. 7002** model mostly collects in the **EF-trimer** while for **Scy. 6803** it leans more toward the **D-trimer**. The majority of the excited-state population remains on the other trimers, in agreement with recent experiments. [42]

Taking into account our error estimations for the lowest-energy pigments, the EET dynamics and excited-state equilibrium are likely more similar than suggested by our simulations. Thus, the equilibrium excited-state population of the TE trimers may be more similar than our results suggest. Nonetheless, these differences may be relevant for explaining why state transitions are different across strains. [21]

4 Conclusions

In this work, we have investigated the energetic landscape of the low-lying excited states in PB cores. We focused on the recent PB atomistic models from two different species, *Synechocystis* PCC 6803 and *Synechococcus* PCC 7002. A combination of structural refinement and multiscale polarizable calculations allowed us to uncover exciton couplings and site energies in the different APC trimers present in PBs.

Our results indicate that the PCBs in the TE trimers (**D-trimer** and **EF-trimer**) are all generally red-shifted with respect to those in the **AB-trimer**. This challenges the simple picture of a few red-shifted bilins in each core, bound to the the ApcE, ApcF, and ApcD proteins.[20,36,37] Instead, the pigments bound to ApcA and ApcB in the TE trimers are also red-shifted. We attributed this to the global and local structural deformations induced in these trimers by the ApcE-linker domain.

We additionally uncovered sensible differences in the site energy ladders calculated from the two PB models, which could be traced back to the different assumptions of symmetry in the atomic reconstruction of the two structures. Notwithstanding this difficulty, we could combine *in silico* mutational analysis and spectroscopy simulations to understand the emission properties of each TE trimer. Furthermore, the spectroscopy simulations helped us assess the inevitable inaccuracies arising from the limited resolution of the atomistic models. We finally showed that our results can reproduce quite well the characteristic time of excitation equilibration in the PB cores.

Our results provide the basis for a more detailed interpretation of time-resolved spectroscopy of phycobilisomes and allow a bottom-up understanding of energy migration and equilibration in the phycobilisome cores.

5 Methods

Structure preparation and refinement. All PB core trimers were extracted from PDB:7EXT (for **Sco. 7002**) and PDB:7SC7 (for **Scy. 6803**). For **Scy. 6803**, we extracted the **AB-trimer** from one of the bottom cylinders (chains CB–CG), plus a second one from the top cylinder (chains CP–CU). Each system was prepared using the `tleap` module of AmberTools18.[43] Amino-acid residues were considered in their standard protonation state, whereas the bilins were modeled with a fully protonated tetrapyrrole backbone, and deprotonated propionic groups. The terminal dihedrals of the Asn and Gln sidechains located close to the pigments were rotated to achieve the lowest-energy conformer. Finally, the D-ring single-bond dihedral N_C=C_{14}-C_{15}=C_{16} of each bilin was set to 180° before minimization. The entire trimer was subject to three restrained minimization stages: first, only bilin pigments and hydrogen atoms were left free to move while the protein's heavy atoms were restrained; second, the side chains within 3 Å of the pigments were also left free to move, while the dihedral between the C and D rings was restrained to 180°; finally, the entire system was minimized without restraints. The Generalized Born GBn[44] continuum solvation model (`igb = 7` in Amber) was used for all minimizations. The ff14SB[45] and GAFF[46] force fields were used for the protein and the bilins, respectively.

QM/MM optimizations. Geometry optimizations of the bilins were performed starting from the refined structure, using the ONIOM scheme[47] with electrostatic embedding as implemented in Gaussian 16.[48] The bilin and the pyrrole-coordinating Asp side chain were treated at the QM B3LYP/6-31G(d) level, whereas the rest of the system was treated with the same force field as in the minimization, and kept frozen. Only the residues within 25 Å of the bilin were considered during the QM/MM optimizations.

Excited-state calculations. Excited-state energies and exciton couplings were computed using the three-layer QM/MMPol/ddCOSMO model[49,50] In the excited-state energy calculations, each bilin pigment was treated at the TD-DFT CAM-B3LYP/6-31G(d) level of theory, whereas the atoms of other bilins and the protein were described as classical point charges and dipole polarizabilities. Finally, a continuum dielectric medium outside of the protein was added and described with the domain-decomposition COSMO (ddCOSMO) model.[51,52] Since this strategy proved successful in describing the excited states of cryptophyte phycobiliproteins,[27] we used the same description in this work. Exciton couplings were computed analytically from the transition densities of the interacting pigments, including the explicit term arising from the presence of a polarizable environment.[53,54] Exciton couplings between bilins belonging to different trimers were computed with the TrEsp method,[35] and appropriately scaled to implicitly account for the environment term. The scaling factor ($s = 0.7$) was determined from the full calculations of within-trimer couplings.

Spectra and energy transfer simulations. Absorption and fluorescence spectra were computed with the cumulant expansion method with the partial ordering prescription (POP),[55] which was later dubbed the "complex Redfield" method.[56] Inhomogeneous broadening was considered by allowing random shifts of the site energies extracted from Gaussian distributions. The spectral density for PCB was taken from the calculations of Ref. 27. To model the trimers lacking ApcD or ApcF, we repeated the simulations shifting the site energy to mimic the substitution of ApcD with ApcA, and of ApcF with ApcB; we used the highest ApcA/ApcB site energy (2.3 eV) to magnify the effect. For the ApcE-CS mutants, the pigment was assumed to be lost and was therefore removed from the exciton system before repeating the simulations. Energy transfer within the PB core was simulated at room temperature using the Generalized Förster method,[57] where the closely associated bilin dimers were treated as exciton domains, whereas all couplings between different bilin dimers were treated perturbatively. The rates within the exciton domains were calculated with Redfield theory. Calculations with standard Förster theory gave EET times of around 50% greater and a similar population evolution. We ignored any decay to the ground state, which occurs on a ns time scale in the unquenched PB.[36]

Conflicts of Interest

There are no conflicts to declare.

Acknowledgement

TK acknowledges the National Research Foundation (NRF), South Africa, Grant No. 137973.

Notes and references

[1] Adir, N., Bar-Zvi, S. & Harris, D. The amazing phycobilisome. *Biochim. Biophys. Acta (BBA) - Bioenergetics* **1861**, 148047 (2020).

[2] Grossman, A. R. A molecular understanding of complementary chromatic adaptation. *Photosynth. Res.* **76**, 207–215 (2003).

[3] Gan, F. *et al.* Extensive remodeling of a cyanobacterial photosynthetic apparatus in far-red light. *Science* **345**, 1312–1317 (2014).

[4] Ho, M.-Y., Gan, F., Shen, G. & Bryant, D. A. Far-red light photoacclimation (FaRLiP) in Synechococcus sp. PCC 7335. II. characterization of phycobiliproteins produced during acclimation to far-red light. *Photosynth. Res.* **131**, 187–202 (2016).

[5] Brejc, K., Ficner, R., Huber, R. & Steinbacher, S. Isolation, crystallization, crystal structure analysis and refinement of allophycocyanin from the cyanobacterium spirulina platensis at 2.3 å resolution. *J. Mol. Biol.* **249**, 424–440 (1995).

[6] Watanabe, M. & Ikeuchi, M. Phycobilisome: architecture of a light-harvesting supercomplex. *Photosynth. Res.* **116**, 265–276 (2013).

[7] Marx, A. & Adir, N. Allophycocyanin and phycocyanin crystal structures reveal facets of phycobilisome assembly. *Biochimica et Biophysica Acta (BBA) - Bioenergetics* **1827**, 311–318 (2013).

[8] Peng, P. P. *et al.* The structure of allophycocyanin B from Synechocystis PCC 6803 reveals the structural basis for the extreme redshift of the terminal emitter in phycobilisomes. *Acta Crystallogr. Sect. D Biol. Crystallogr.* **70**, 2558–2569 (2014).

[9] Tang, K. *et al.* The terminal phycobilisome emitter, L CM : A light-harvesting pigment with a phytochrome chromophore. *Proc. Natl. Acad. Sci.* **112**, 15880–15885 (2015).

[10] Bar-Zvi, S. *et al.* Structural heterogeneity leads to functional homogeneity in a. marina phycocyanin. *Biochim. Biophys. Acta (BBA) - Bioenerg.* **1859**, 544–553 (2018).

[11] Gwizdala, M., Krüger, T. P. J., Wahadoszamen, M., Gruber, J. M. & van Grondelle, R. Phycocyanin: One complex, two states, two functions. *J. Phys. Chem. Lett.* **9**, 1365–1371 (2018).

[12] MacColl, R. Allophycocyanin and energy transfer. *Biochim. Biophys. Acta (BBA) - Bioenerg.* **1657**, 73–81 (2004).

[13] Domínguez-Martín, M. A. *et al.* Structures of a phycobilisome in light-harvesting and photoprotected states. *Nature* **609**, 835–845 (2022).

[14] Zheng, L. *et al.* Structural insight into the mechanism of energy transfer in cyanobacterial phycobilisomes. *Nat. Commun.* **12**, 5497 (2021).

[15] Liu, H. *et al.* Structure of cyanobacterial phycobilisome core revealed by structural modeling and chemical cross-linking. *Sci. Adv.* **7**, eaba5743 (2021). URL http://dx.doi.org/10.1126/sciadv.aba5743.

[16] Holzwarth, A. R., Bittersmann, E., Reuter, W. & Wehrmeyer, W. Studies on chromophore coupling in isolated phycobiliproteins. *Biophys. J.* **57**, 133–145 (1990).

[17] McGregor, A., Klartag, M., David, L. & Adir, N. Allophycocyanin trimer stability and functionality are primarily due to polar enhanced hydrophobicity of the phycocyanobilin binding pocket. *J. Mol. Biol.* **384**, 406–421 (2008).

[18] Gindt, Y. M., Zhou, J., Bryant, D. A. & Sauer, K. Spectroscopic studies of phycobilisome subcore preparations lacking key core chromophores: Assignment of excited state energies to the Lcm, β18 and αAP-B chromophores. *Biochim. Biophys. Acta - Bioenerg.* **1186**, 153–162 (1994).

[19] Ashby, M. K. & Mullineaux, C. W. *Photosynth. Res.* **61**, 169–179 (1999). URL http://dx.doi.org/10.1023/A:1006217201666.

[20] Jallet, D., Gwizdala, M. & Kirilovsky, D. ApcD, ApcF and ApcE are not required for the Orange Carotenoid Protein related phycobilisome fluorescence quenching in the cyanobacterium Synechocystis PCC 6803. *Biochim. Biophys. Acta - Bioenerg.* **1817**, 1418–1427 (2012).

[21] Calzadilla, P. I., Muzzopappa, F., Sétif, P. & Kirilovsky, D. Different roles for ApcD and ApcF in Synechococcus elongatus and Synechocystis sp. PCC 6803 phycobilisomes. *Biochim. Biophys. Acta - Bioenerg.* **1860**, 488–498 (2019).

[22] Renger, T. & Müh, F. Understanding photosynthetic light-harvesting: a bottom up theoretical approach. *Phys. Chem. Chem. Phys.* **15**, 3348 (2013).

[23] Cupellini, L., Bondanza, M., Nottoli, M. & Mennucci, B. Successes & challenges in the atomistic modeling of light-harvesting and its photoregulation. *Biochim. Biophys. Acta - Bioenerg.* **1861**, 148049 (2020).

[24] Cignoni, E., Slama, V., Cupellini, L. & Mennucci, B. The atomistic modeling of light-harvesting complexes from the physical models to the computational protocol. *J. Chem. Phys.* **156**, 120901 (2022).

[25] Lee, M. K., Bravaya, K. B. & Coker, D. F. First-Principles Models for Biological Light-Harvesting: Phycobiliprotein Complexes from Cryptophyte Algae. *J. Am. Chem. Soc.* **139**, 7803–7814 (2017).

[26] Blau, S. M., Bennett, D. I. G., Kreisbeck, C., Scholes, G. D. & Aspuru-Guzik, A. Local protein solvation drives direct down-conversion in phycobiliprotein PC645 via incoherent vibronic transport. *Proc. Natl. Acad. Sci.* **115**, E3342–E3350 (2018).

[27] Corbella, M., Cupellini, L., Lipparini, F., Scholes, G. D. & Curutchet, C. Spectral Variability in Phycocyanin Cryptophyte Antenna Complexes is Controlled by Changes in the α-Polypeptide Chains. *ChemPhotoChem* **3**, 945–956 (2019).

[28] Womick, J. M. & Moran, A. M. Vibronic Enhancement of Exciton Sizes and Energy Transport in Photosynthetic Complexes. *J. Phys. Chem. B* **115**, 1347–1356 (2011).

[29] Müh, F., Madjet, M. E.-A. & Renger, T. Structure-Based Identification of Energy Sinks in Plant Light-Harvesting Complex II. *J. Phys. Chem. B* **114**, 13517–13535 (2010).

[30] Jurinovich, S., Viani, L., Prandi, I. G., Renger, T. & Mennucci, B. Towards an ab initio description of the optical spectra of light-harvesting antennae: application to the CP29 complex of photosystem II. *Phys. Chem. Chem. Phys.* **17**, 14405–16 (2015).

[31] Soulier, N. & Bryant, D. A. The structural basis of far-red light absorbance by allophycocyanins. *Photosynth. Res.* **147**, 11–26 (2021).

[32] Macaluso, V., Salvadori, G., Cupellini, L. & Mennucci, B. The structural changes in the signaling mechanism of bacteriophytochromes in solution revealed by a multiscale computational investigation. *Chem. Sci.* **12**, 5555–5565 (2021).

[33] Gwizdala, M., Wilson, A. & Kirilovsky, D. In vitro reconstitution of the cyanobacterial photoprotective mechanism mediated by the orange carotenoid protein in synechocystis pcc 6803. *Plant Cell* **23**, 2631–2643 (2011).

[34] Assefa, G. T. *et al.* ApcE plays an important role in light-induced excitation energy dissipation in the synechocystis PCC6803 phycobilisomes. *Photosynth. Res.* DOI: 10.1007/s11120–024–01078–6 (2024).

[35] Madjet, M. E., Abdurahman, A. & Renger, T. Intermolecular coulomb couplings from ab initio electrostatic potentials: application to optical transitions of strongly coupled pigments in photosynthetic antennae and reaction centers. *J. Phys. Chem. B* **110**, 17268–17281 (2006).

[36] van Stokkum, I. H. *et al.* A functional compartmental model of the Synechocystis PCC 6803 phycobilisome. *Photosynth. Res.* **135**, 87–102 (2018).

[37] Biswas, A., Akhtar, P., Lambrev, P. H. & van Stokkum, I. H. Energy transfer from phycobilisomes to photosystem i at room temperature. *Front. Plant Sci.* **14**, 1300532 (2024).

[38] Wang, Q. & Moerner, W. E. Dissecting pigment architecture of individual photosynthetic antenna complexes in solution. *Proc. Natl. Acad. Sci. U. S. A.* **112**, 13880–13885 (2015).

[39] Tian, L. *et al.* Picosecond Kinetics of Light Harvesting and Photoprotective Quenching in Wild-Type and Mutant Phycobilisomes Isolated from the Cyanobacterium Synechocystis PCC 6803. *Biophys. J.* **102**, 1692–1700 (2012).

[40] Gisriel, C. J. *et al.* Structural comparison of allophycocyanin variants reveals the molecular basis for their spectral differences. *Photosynth. Res.* DOI: 10.1007/s11120–023–01048–4 (2023).

[41] Gisriel, C. J. *et al.* Helical allophycocyanin nanotubes absorb far-red light in a thermophilic cyanobacterium. *Sci. Adv.* **9**, eadg0251 (2023).

[42] Sohoni, S. *et al.* Phycobilisome's exciton transfer efficiency relies on an energetic funnel driven by chromophore–linker protein interactions. *J. Am. Chem. Soc.* **145**, 11659–11668 (2023).

[43] Case, D. A. *et al.* Amber 2018 (2018). University of California, San Francisco.

[44] Mongan, J., Simmerling, C., McCammon, J. A., Case, D. A. & Onufriev, A. Generalized born model with a simple, robust molecular volume correction. *J. Chem. Theory Comput.* **3**, 156–169 (2007).

[45] Maier, J. A. *et al.* ff14sb: Improving the accuracy of protein side chain and backbone parameters from ff99sb. *J. Chem. Theory Comput.* **11**, 3696–3713 (2015).

[46] Wang, J., Wolf, R. M., Caldwell, J. W., Kollman, P. a. & Case, D. a. Development and testing of a general amber force field. *J. Comput. Chem.* **25**, 1157–1174 (2004).

[47] Chung, L. W. *et al.* The ONIOM method and its applications. *Chem. Rev.* **115**, 5678–5796 (2015).

[48] Frisch, M. J. *et al.* Gaussian 16 Revision C.01 (2016). Gaussian Inc. Wallingford CT.

[49] Lipparini, F. *et al.* Quantum, classical, and hybrid QM/MM calculations in solution: General implementation of the ddCOSMO linear scaling strategy. *J. Chem. Phys.* **141**, 184108 (2014).

[50] Nottoli, M., Nifosì, R., Mennucci, B. & Lipparini, F. Energy, structures, and response properties with a fully coupled QM/AMOEBA/ddCOSMO implementation. *J. Chem. Theory Comput.* **17**, 5661–5672 (2021).

[51] Lipparini, F., Stamm, B., Cancès, E., Maday, Y. & Mennucci, B. Fast domain decomposition algorithm for continuum solvation models: Energy and first derivatives. *J. Chem. Theory Comput.* **9**, 3637–3648 (2013).

[52] Lipparini, F. *et al.* Quantum calculations in solution for large to very large molecules: A new linear scaling QM/continuum approach. *J. Phys. Chem. Lett.* **5**, 953–958 (2014).

[53] Curutchet, C. *et al.* Electronic Energy Transfer in Condensed Phase Studied by a Polarizable QM/MM Model. *J. Chem. Theory Comput.* **5**, 1838–1848 (2009).

[54] Cupellini, L., Corbella, M., Mennucci, B. & Curutchet, C. Electronic energy transfer in biomacromolecules. *WIREs Comput. Mol. Sci.* **9**, e1392 (2019).

[55] Renger, T. & Marcus, R. A. On the relation of protein dynamics and exciton relaxation in pigment–protein complexes: An estimation of the spectral density and a theory for the calculation of optical spectra. *J. Chem. Phys.* **116**, 9997–10019 (2002).

[56] Gelzinis, A., Abramavicius, D. & Valkunas, L. Absorption lineshapes of molecular aggregates revisited. *J. Chem. Phys.* **142**, 154107 (2015).

[57] Yang, M., Damjanović, A., Vaswani, H. M. & Fleming, G. R. Energy transfer in photosystem i of cyanobacteria synechococcus elongatus: Model study with structure-based semi-empirical hamiltonian and experimental spectral density. *Biophys. J.* **85**, 140–158 (2003).